

Application of Hertz vector diffraction theory to the diffraction of focused Gaussian beams and calculations of focal parameters

Glen D. Gillen¹, Kendra Baughman¹, and Shekhar Guha²

¹Physics Department, California Polytechnic State University,
San Luis Obispo, CA, 93407, USA

²Air Force Research Laboratory, Materials and Manufacturing Directorate,
Wright-Patterson Air Force Base, Dayton, OH, 45433, USA

ggillen@calpoly.edu

Abstract: Hertz vector diffraction theory is applied to a focused TEM₀₀ Gaussian light field passing through a circular aperture. The resulting theoretical vector field model reproduces plane-wave diffractive behavior for severely clipped beams, expected Gaussian beam behavior for unperturbed focused Gaussian beams as well as unique diffracted-Gaussian behavior between the two regimes. The maximum intensity obtainable and the width of the beam in the focal plane are investigated as a function of the clipping ratio between the aperture radius and the beam width in the aperture plane.

© 2009 Optical Society of America

OCIS codes: (050.1220) apertures; (050.1960) Diffraction theory; (220.2560) propagating methods

References and links

1. G. R. Kirchhoff, "Zur Theorie der Lichtstrahlen," *Ann. Phys. (Leipzig)* **18**, 663-695 (1883).
2. A. Sommerfeld, "Zur mathematischen Theorie der Beugungerscheinungen," *Nachr. Kgl. Wiss Göttingen* **4**, 338-342 (1894).
3. Lord Rayleigh, "On the passage of waves through apertures in plane screens, and allied problems," *Philos. Mag.* **43**, 259-272 (1897).
4. S. Guha and G. D. Gillen, "Description of light propagation through a circular aperture using nonparaxial vector diffraction theory," *Opt. Express* **13**, 1424-1447 (2005).
5. G. D. Gillen, S. Guha, and K. Christandl, "Optical dipole traps for cold atoms using diffracted laser light," *Phys. Rev. A* **73**, 013409 (2006).
6. S. Guha and G. D. Gillen, "Vector diffraction theory of refraction of light by a spherical surface," *J. Opt. Soc. Am. B* **24**, 1-8 (2007).
7. W. Hsu and R. Barakat, "Stratton-Chu vectorial diffraction of electromagnetic fields by apertures with application to small-Fresnel-number systems," *J. Opt. Soc. Am. A* **11**, 623-629 (1994).
8. Y. Li, "Focal shifts in diffracted converging electromagnetic waves. I. Kirchhoff theory," *J. Opt. Soc. Am. A* **22**, 68-76 (2005).
9. Y. Li, "Focal shifts in diffracted converging electromagnetic waves. II. Rayleigh theory," *J. Opt. Soc. Am. A* **22**, 77-83 (2005).
10. K. Duan and B. Lü, "Vectorial nonparaxial propagation equation of elliptical Gaussian beams in the presence of a rectangular aperture," *J. Opt. Soc. Am. A* **21**, 1613-1620 (2004).
11. B. Lü and K. Duan, "Nonparaxial propagation of vectorial Gaussian beams diffracted at a circular aperture," *Opt. Lett.* **28**, 2440-2442 (2003).
12. G. Zhou, "The analytical vectorial structure of a nonparaxial Gaussian beam close to the source," *Opt. Express* **16**, 3504-3514 (2008).

13. K. Duan and B. Lü, "Polarization properties of vectorial nonparaxial Gaussian beams in the far field," *Opt. Lett.* **2005**, 308–310 (2005).
14. C. G. Chen, P. T. Konkola, J. Ferrera, R. K. Heilmann, and M. L. Schattenburg, "Analyses of vector Gaussian beam propagation and the validity of paraxial and spherical approximations," *J. Opt. Soc. Am. A* **19**, 404–412 (2002).
15. G. P. Agrawal and D. N. Pattanayak, "Gaussian beam propagation beyond the paraxial approximation," *J. Opt. Soc. Am.* **69**, 575–578 (1979).
16. G. D. Gillen and S. Guha, "Modeling and propagation of near-field diffraction patterns: a more complete approach," *Am. J. Phys.* **72**, 1195–1201 (2004).
17. M. Born and E. Wolf, *Principles of Optics* (Cambridge University Press, Cambridge, 2003.)
18. M. S. Yeung, "Limitation of the Kirchhoff boundary conditions for aerial image simulations in 157-nm optical lithography," *IEEE Electron. Dev. Lett.* **21**, 433–435 (2000).
19. G. Bekefi, "Diffraction of electromagnetic waves by an aperture in a large screen," *J. Appl. Phys.* **24**, 1123–1130 (1953).
20. W. H. Carter, "Electromagnetic field of a Gaussian beam with an elliptical cross section," *J. Opt. Soc. Am.* **62**, 1195–1201 (1972).
21. D. R. Rhodes, "On a fundamental principle in the theory of planar antennas," *Proc. IEEE* **52**, 1013–1021 (1964).
22. D. R. Rhodes, "On the stored energy of planar apertures," *IEEE Trans. Antennas Propag.* **AP-14**, 676–683 (1966).
23. I. Ghebregziabher and B. C. Walker, "Effect of focal geometry on radiation from atomic ionization in an ultra-strong and ultrafast laser field," *Phys. Rev. A* **76**, 023415 (2007).
24. J. M. P. Coelho, M. A. Abreu, and F. C. Rodrigues, "Modelling the spot shape influence on high-speed transmission lap welding of thermoplastic films," *J. Opt. Lasers Eng.* **46**, 55–61 (2007).
25. A. Yariv, *Quantum Electronics*, Third Edition, (John Wiley & Sons, New York, 1989.)

1. Introduction

The passage of electromagnetic fields through structures and apertures has been investigated and modeled for well over a hundred years [1–3]. The continual increase in computer speed over the past decade has led to accurate and detailed solutions of the electromagnetic diffraction equation [4–11]. Modeling of Gaussian beam propagation under a variety of conditions has also been an active field of study [12–15], especially because laser resonator structures are usually configured to produce output beams that are Gaussian in transverse spatial dimensions.

When the values of the electromagnetic fields of the light wave are known in a plane, diffraction theory is used to describe the propagation of light to other points. Diffraction theory is usually applied when the transmission of the incident light field through the input plane is spatially limited due to a finite aperture in an otherwise opaque plane.

One common choice for the input light field for various vector diffraction theories is that of a plane wave [4–7]. Theoretically, plane waves are chosen for their mathematical simplicity. Experimentally, localized "plane waves" are typically created by placing an aperture in the path of a laser beam (where the aperture radius is much smaller than the beam width in the aperture plane) creating a virtually uniform field within the aperture. Other input light fields used have been converging spherical waves [8, 9], and collimated Gaussian beams [10, 11]. Differences between one diffraction model and another are found in the choices of the diffraction integrals and the input parameters; each of which can limit the region of validity of the model.

Diffraction theory developed by Rayleigh, Sommerfeld and others [2, 3, 10, 11, 16] use Kirchhoff boundary conditions [17] which use a chosen electromagnetic field in the aperture plane as the input parameter. However, description of light propagation from an open aperture in an opaque plane screen using the Rayleigh-Sommerfeld theory is complicated by the fact that the net field values in the aperture plane are not known *a priori*. When Kirchhoff boundary conditions are invoked, which assume that the field values in the opening of an aperture are the same as that obtained in the absence of the screen and zero elsewhere in the input plane, Maxwell's equations are not satisfied in the aperture plane and regions very close to the aperture because the fields are discontinuous. In addition to not satisfying Maxwell's equations, the solutions are not physically meaningful near the aperture plane as they do not include any

perturbations to the input field due to scattering effects of the aperture boundary [18]. Experimentally measured values of electromagnetic fields in the aperture plane for incident plane waves [19] show strong perturbations to the incident electromagnetic fields, which do not conform with predictions based on Rayleigh-Sommerfeld diffraction theory. Thus, if the chosen input fields do not explicitly obey Maxwell's equations and include perturbation effects due to the aperture edge then the use of Rayleigh-Sommerfeld models are invalid near the aperture plane.

Hertz vector diffraction theory (HVDT) uses a vector potential as the known input parameter. (For a discussion on Hertz vectors and their relationships to the electric and magnetic fields see section 2.2.2 of ref. [17].) The vector potential is chosen to be one which satisfies the wave equation, and reproduces the incident electromagnetic field as it would exist in the absence of the aperture. Care must be taken such that the chosen vector potential satisfies Maxwell's equations. The choices for accurate input field parameters are an easier task using HVDT than when using Kirchhoff boundary conditions. The Hertz vector diffraction input is the vector potential of just the incident field; whereas the input field choice using Kirchhoff boundary conditions assumes the *net* electromagnetic fields in the aperture region are already known. Using HVDT the net electromagnetic fields within the aperture plane are not assumed to be known, but rather they are calculated through Maxwell's equations from a diffracted vector potential. Thus electromagnetic field values calculated using HVDT inherently satisfy Maxwell's equations everywhere. It has been previously shown by Bekefi [19] that calculations using HVDT match experimentally measured electromagnetic field distributions in and near the aperture plane, including all perturbations to the net fields due to scattering and the aperture itself. Based upon Bekefi's treatment of the diffraction model, we have shown that using a suitable choice of the vector potential function for a plane wave incident upon an aperture allows for the calculation of the field values at other points [4].

The Gaussian properties of the output of most laser systems have been one of the driving forces for current research efforts to model the propagation of non-paraxial vectorial Gaussian beams. Many of these research efforts [12–15] use the angular spectrum representation for the propagation of non-diffracted Gaussian beams, pioneered by Carter [20] and Rhodes [21, 22]. Some fields of study, ranging from fundamental atomic physics [23] to industrial laser welding [24], are primarily concerned with two important parameters of focused Gaussian beams: maximum attainable intensity, and minimum attainable spot size. For a given physical focusing optic, higher peak intensities and smaller minimum spot sizes for Gaussian beams are obtained by enlarging the beam width incident upon the optic. Experimentally, there has always been a trade off between the size of the incident beam and how much of the wings of the incident beam are “clipped” by the physically limited size of the focusing optic. In addition to focusing optical components, ‘apertures’ can occur in the form of beam steering mirrors, entrance pupils or windows to vacuum chambers, sample mounts, enclosures, etc. To the best of the authors' knowledge, empirical relationships of the dependence of the peak intensity and minimum focal spot width on the clipping parameter of optical components currently do not exist.

Here we extend HVDT to the case of an incident focused Gaussian beam (GHVDT). The cases of interest include the modifications to the transverse profile of the beam by the aperture in the near-aperture regions, and the modifications to the focusing characteristics of the beam by the aperture for various ratios of the aperture size to the incident Gaussian beam radius. The theoretical model is presented for an incident TEM₀₀ Gaussian beam with the focal plane independent of the aperture plane, allowing the model to be used for either converging or diverging incident Gaussian beams. Thus, the method presented can function as a single theoretical model for near and far-field diffraction, for propagation of either converging or diverging Gaussian beams, or for propagation of converging or diverging diffracted-Gaussian beams.

2. Theory

The vector electromagnetic fields, \mathbf{E} and \mathbf{H} , of a propagating light field can be determined from a vector polarization potential, Π , using [19, 17]

$$\mathbf{E} = k^2\Pi + \nabla(\nabla \cdot \Pi), \quad (1)$$

and

$$\mathbf{H} = ik\sqrt{\frac{\epsilon_o}{\mu_o}}\nabla \times \Pi. \quad (2)$$

where $k = 2\pi/\lambda$ is the wave number, and ϵ_o and μ_o are the permittivity and permeability of free space, respectively. The vector potential Π , also known as the Hertz vector [17], must satisfy the wave equation at all points in space.

In HVDT, a Hertz vector for the incident field, Π_i , is chosen at a plane and then the Hertz vector beyond the diffraction surface, Π , is determined from the propagation of the incident vector field using Neumann boundary conditions [19]. The complete six-component electromagnetic field can be determined from the x -component of the Hertz vector at the point of interest beyond the aperture plane, and is given by [19]

$$\Pi_x(\mathbf{r}) = -\frac{1}{2\pi} \iint_{z_o=0} \left(\frac{\partial \Pi_{ix}(\mathbf{r}_o)}{\partial z_o} \right) \frac{e^{-ik\rho}}{\rho} dx_o dy_o. \quad (3)$$

where \mathbf{r} is a function of the coordinates of the point of interest beyond the aperture plane, (x, y, z) , \mathbf{r}_o is a source point in the diffraction plane, (x_o, y_o, z_o) , and

$$\rho = |\mathbf{r} - \mathbf{r}_o|. \quad (4)$$

The limits of integration of Eq. (3) are the limits of the open area in the aperture plane. The complete \mathbf{E} and \mathbf{H} vector fields at the point of interest are then determined by substitution of Eq. (3) into Eqs. (1) and (2).

The x -component of an incident Gaussian electric field polarized in the x -dimension can be written as [25]

$$E_{ix}(\mathbf{r}_o) = E_o \exp \left[-i \left(-i \ln \left(1 + \frac{z_o}{q_o} \right) + \frac{kr_o^2}{2(q_o + z_o)} + kz_o \right) \right], \quad (5)$$

or equivalently,

$$E_{ix}(\mathbf{r}_o) = \frac{E_o}{\left(1 + \frac{z_o}{q_o} \right)} \exp \left[-\frac{ikr_o^2}{2(q_o + z_o)} - ikz_o \right], \quad (6)$$

where

$$q_o = i\frac{k}{2}w_o^2, \quad (7)$$

$$r_o^2 = x_o^2 + y_o^2, \quad (8)$$

and w_o is the e^{-1} minimum half-width of the incident electric field.

The Hertz vector of the incident field of a Gaussian laser beam with the minimum beam waist located at $z = z_G$ can be chosen as

$$\Pi_{ix}(\mathbf{r}_o) = \frac{E_o}{k^2} \frac{1}{\left(1 + \frac{z_o - z_G}{q_o} \right)} \exp \left[-\frac{ikr_o^2}{2(q_o + z_o - z_G)} - ik(z_o - z_G) \right]. \quad (9)$$

The normal partial derivative of the incident Hertz vector evaluated in the aperture plane becomes

$$\left(\frac{\partial \Pi_{ix}}{\partial z_o}\right)_{z_o=0} = \frac{E_o}{k^2} A(x_o, y_o) \quad (10)$$

where

$$A(x_o, y_o) = \frac{1}{1 - \frac{z_G}{q_o}} \left(\frac{ikr_o^2}{2(q_o - z_G)^2} - \frac{1}{q_o - z_G} - ik \right) \exp\left(\frac{-ikr_o^2}{2(q_o - z_G)}\right). \quad (11)$$

Substitution of Eqs. (11) and (10) into Eq. (3) yields the Hertz vector at the point of interest. The components of the electromagnetic field at the point of interest are determined by substitution of Eq. (3) into Eqs. (1) and (2), yielding

$$\begin{aligned} E_x &= k^2 \Pi_x + \frac{\partial^2 \Pi_x}{\partial x^2}, \\ E_y &= \frac{\partial^2 \Pi_x}{\partial y \partial x}, \\ E_z &= \frac{\partial^2 \Pi_x}{\partial z \partial x}, \end{aligned} \quad (12)$$

and

$$\begin{aligned} H_x &= 0, \\ H_y &= ik \sqrt{\frac{\epsilon_o}{\mu_o}} \frac{\partial \Pi_x}{\partial z}, \\ H_z &= -ik \sqrt{\frac{\epsilon_o}{\mu_o}} \frac{\partial \Pi_x}{\partial y}. \end{aligned} \quad (13)$$

It is computationally convenient to express all of the parameters in dimensionless form. To do so, all tangential distances and parameters are normalized to the minimum beam waist, ω_o , and all axial distances and parameters are normalized to a quantity $z_n \equiv k\omega_o^2 = p_1\omega_o$, where the parameter p_1 is defined as $p_1 = k\omega_o$. All normalized variables, parameters, and functions are denoted with a subscript "1". The normalized variables and parameters are

$$x_1 \equiv \frac{x}{\omega_o}, \quad y_1 \equiv \frac{y}{\omega_o}, \quad z_1 \equiv \frac{z}{z_n}, \quad (14)$$

$$x_{o1} \equiv \frac{x_o}{\omega_o}, \quad y_{o1} \equiv \frac{y_o}{\omega_o}, \quad z_{G1} \equiv \frac{z_G}{z_n}, \quad \text{and} \quad q_1 \equiv \frac{q_o}{z_n}. \quad (15)$$

Substitution of Eqs. (11) & (10) into (3) and (3) into Eqs. (12) & (13), carrying out the differentiations, and using normalized variables and functions, the electric and magnetic fields at the point of interest can be expressed as

$$E_x(\mathbf{r}_1) = -\frac{E_o}{2\pi p_1} \iint A_1 f_1 \left[(1 + s_1) - (1 + 3s_1) \frac{(x_1 - x_{o1})^2}{\rho_1^2} \right] dx_{o1} dy_{o1}, \quad (16)$$

$$E_y(\mathbf{r}_1) = \frac{E_o}{2\pi p_1} \iint A_1 f_1 (1 + 3s_1) \frac{(x_1 - x_{o1})(y_1 - y_{o1})}{\rho_1^2} dx_{o1} dy_{o1}, \quad (17)$$

$$E_z(\mathbf{r}_1) = \frac{E_o z_1}{2\pi} \iint A_1 f_1 (1 + 3s_1) \frac{(x_1 - x_{o1})}{\rho_1^2} dx_{o1} dy_{o1}, \quad (18)$$

and

$$H_x(\mathbf{r}_1) = 0, \quad (19)$$

$$H_y(\mathbf{r}_1) = -\frac{ip_1 z_1 H_0}{2\pi} \iint A_1 f_1 s_1 dx_{01} dy_{01}, \quad (20)$$

$$H_z(\mathbf{r}_1) = \frac{iH_0}{2\pi} \iint A_1 f_1 s_1 (y_1 - y_{01}) dx_{01} dy_{01}, \quad (21)$$

where

$$A_1 = \frac{1}{1 + 2iz_{G1}} \left(\frac{ir_{01}^2}{2(q_1 - z_{G1})^2} - \frac{1}{(q_1 - z_{G1})} - ip_1^2 \right) \exp\left(\frac{-ir_{01}^2}{2(q_1 - z_{G1})}\right), \quad (22)$$

$$f_1 = \frac{e^{-ip_1 \rho_1}}{\rho_1}, \quad (23)$$

$$s_1 = \frac{1}{ip_1 \rho_1} \left(1 + \frac{1}{ip_1 \rho_1} \right), \quad (24)$$

$$\rho_1^2 = (x_1 - x_{01})^2 + (y_1 - y_{01})^2 + p_1^2 z_1^2, \quad (25)$$

and

$$r_{01}^2 = x_{01}^2 + y_{01}^2. \quad (26)$$

3. Calculations of light fields

The equations derived above are applied to a practical case of apertured Gaussian laser beam propagation. A Gaussian laser beam (TEM₀₀ mode) having a wavelength of 780 nm is focused to a spot size ω_o (e^{-1} Gaussian half width of the electric field) of 5 μm . The Rayleigh range, $z_R = \pi\omega_o^2/\lambda$, for this beam is 100.7 μm . Figure 1 illustrates the theoretical setup for the calculations conducted using GHVDT. The focused beam is incident upon the aperture and propagating in the $+z$ direction. The origin of the coordinate system is at the center of a circular aperture placed normal to the beam such that the center of the aperture coincides with the center of the beam. For the GHVDT presented in this manuscript, the parameter z_G is left as an independent variable such that the axial location of the unperturbed focal plane is independent with respect to the location of the aperture plane. The beam waist in the aperture plane is ω_a , and determined by [25]

$$\omega_a^2 = \omega_o^2 \left(1 + \frac{z_G^2}{z_R^2} \right). \quad (27)$$

By allowing z_G to remain an independent variable, calculations can be performed for the focal plane before, coplanar, or after the aperture plane depending upon the value used for z_G .

Three regimes are studied in this investigation: (1) pure Gaussian behavior where the incident beam is unperturbed by the aperture size, or $a \gg \omega_a$, (2) pure diffraction behavior where the incident beam is highly clipped, or $a \ll \omega_a$, and (3) the diffracted-Gaussian regime where $a < \omega_a \approx a$.

The regime where the radius of the aperture is significantly larger than the beam width in the aperture plane corresponds to a regime where a Gaussian beam is expected to continue behaving as an unperturbed Gaussian beam. Under these conditions, the physical aperture or optic is significantly larger than the beam, and an incident focused Gaussian TEM₀₀ will continue through the aperture as an unperturbed TEM₀₀ beam. To model this regime, an a/ω_a ratio of 4 is chosen, where for a centered beam, the relative intensity at the edge of the the aperture is

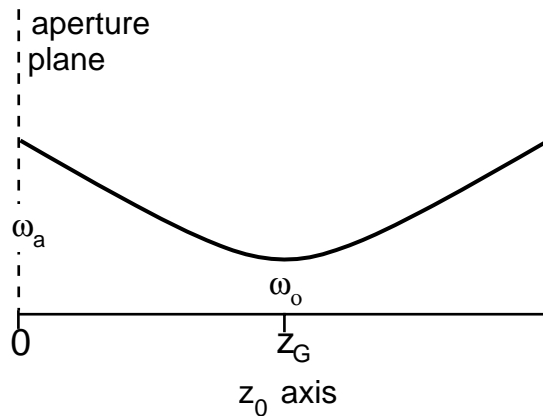


Fig. 1. Theoretical setup for most calculations, where ω_a is the e^{-1} width of the electric field of the incident Gaussian field in the aperture plane, ω_o is the minimum beam waist, and z_G is the on-axis location of the Gaussian focal plane.

$\sim 10^{-14}$. Calculations using the GHVDT model presented here are directly compared to calculations using a purely Gaussian beam propagation model presented by Yariv in section 6.6 of reference [25] (henceforth referred to as the “Yariv” model.)

Figure 2 is a collection of calculations of the relative intensity of the light field for $a = 4\omega_a$ using the complete GHVDT outlined previously, and using the purely Gaussian Yariv model. The intensity calculated in the plots, S_z/S_o , is the normalized z -component of the Poynting vector of the electromagnetic fields. All intensities of Fig.2 are normalized to the peak intensity in the focal plane. Figures 2(a) and (b) are calculations where $z_G = 0$, or the focal plane is coplanar with the aperture plane. When the focal plane is coplanar with the aperture plane, calculations for the intensity versus radial position, Fig. 2(a), reproduce the unperturbed incident Gaussian beam using the Yariv model in the aperture plane. Figure 2(b) shows that the calculated on-axis intensity for axial positions beyond the aperture plane using GHVDT also reproduce the expected axial behavior for diverging TEM₀₀ purely Gaussian beams.

Figures 2(c) and (d) are calculations for $z_G = 0.01$ m, where the focal plane is located 1 cm beyond the aperture plane. The incident Hertz vector (Eq. 9) in the aperture plane is one which yields a converging focused Gaussian beam with a width in the aperture plane which follows that of Eq. (27), or $\omega_a = 99\omega_o$, and the normalized peak intensity in the aperture plane is 1×10^{-4} . Using the full GHVDT and a z_G value of 1 cm, Fig. 2(c) is a calculation of the normalized intensity versus radial position for a distance of 1 cm beyond the aperture plane. Note that calculations using GHVDT for the regime of $a \ll \omega_a$ reproduce calculated behavior using the Yariv model. For an unperturbed converging Gaussian beam, the on-axis intensity is expected to follow a Lorentzian function with an offset maximum occurring at the axial location of the focal plane, and having a normalized intensity of 1. Using GHVDT and input parameters of $z_G = 0.01$ m and $a = 4\omega_a$, the expected on-axis Gaussian behavior is reproduced, as illustrated in Fig. 2(d).

For the pure diffraction regime, the parameters chosen are $z_G = 0.01$ m, and values of $a/\omega_a < 0.016$. For these values of a/ω_a , the variation between the intensity at the center of the aperture and the edge of the aperture is less than 0.05%. Thus the incident Hertz vector in the aperture region is virtually uniform, and calculations using GHVDT should reproduce those for a plane wave incident upon a circular aperture. Thus, the model chosen for comparison is that of Hertz vector diffraction theory, HVDT, applied to the diffraction of a plane wave incident upon a

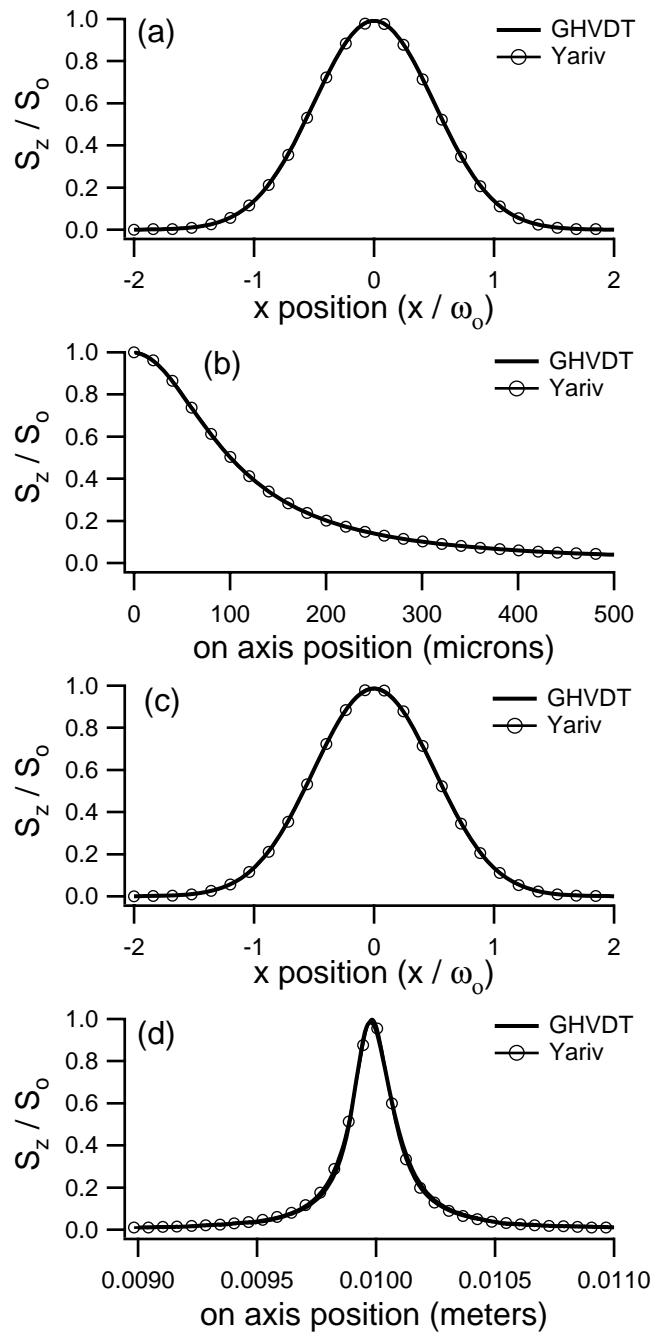


Fig. 2. Calculated Gaussian behavior for $a/\omega_a = 4$ using GHVDT. Figures (a) and (b) are the normalized intensity versus x in the aperture plane and versus z , respectively, for $z_G = 0$. Figures (c) and (d) are the normalized intensity versus x in the focal plane and versus z , respectively, for $z_G = 0.01$ m. Calculated intensity distributions using a purely Gaussian beam propagation model, Yariv, are included for comparison purposes.

circular aperture [4]. For a complete description of HVDT applied to a plane wave incident upon a circular aperture and comparisons of that model to other vector diffraction models see ref. [4]. An important parameter in the pure diffraction regime is the ratio of the aperture radius to the wavelength of the light, a/λ . According to HVDT applied to plane wave diffraction, the on-axis intensity will oscillate as a function of increasing axial distance. The number of oscillations of the on-axis intensity will be equal to the a/λ ratio [4]. The maximum on-axis intensity will have a value of 4 times the normalized incident intensity and will be located at a position of $z = a^2/\lambda$. In the aperture plane, the central intensity will modulate about the normalized incident intensity value as a function of the aperture to wavelength ratio due to scattering effects of the aperture edge [19]. Modulations in the fields within the aperture plane were both experimentally measured and calculated using HVDT by Bekefi in 1953 [19]. The intensity value at the center of the aperture plane will be a maximum for integer values of the a/λ ratio, and will be a minimum for half integer values. Using HVDT, the z -component of the Poynting vector at the center of the aperture will have a normalized maximum value in the aperture plane of 1.5 and a minimum value of 0.5 [4].

Figure 3 is a calculation of the normalized on-axis z -component of the Poynting vector using GHVDT for a/λ ratios of (a) 5, (b) 5.5, and (c) 10, and an unperturbed focal plane location of $z_G = 0.01$ m. Note that the intensity is normalized to the expected peak Gaussian intensity in the focal plane of an unperturbed beam, which makes the normalized intensity incident upon the aperture 10^{-4} . Figure 3 also includes plots for the calculated on-axis intensity distributions according to HVDT of a plane wave incident upon a circular aperture. Note that all aspects of the calculations in Fig. 3 for a highly clipped, converging, focused Gaussian beam reproduce those expected for the diffraction of a plane wave even though the GHVDT still contains all of the phase information for a converging focused Gaussian TEM₀₀ within input light field.

In the diffracted-Gaussian regime, the a/ω_a ratio enters the region of ~ 0.1 to ~ 1 , and the behavior of the light field within and beyond the aperture plane is neither pure diffractive behavior nor pure Gaussian behavior. This is a regime where traditional diffraction models and Gaussian beam propagation models are invalid. To the best of the authors' knowledge, no vector diffraction theory exists in the literature for a focused diffracted-Gaussian beam. Thus, comparison of light field distributions for the model presented here to other vector diffraction models is currently not possible. An example of a calculation only possible with the GHVDT presented here is the normalized intensity illustrated in Fig. 4. Figure 4 is the z -component of the Poynting vector as a function of both x and y in the aperture plane for the focal plane coplanar with the aperture plane ($z_G = 0$), an aperture radius of $a = 5\lambda = 0.78\omega_o$, and the polarization of the incident light along the x -axis. For an a/ω_a ratio of 0.78, the intensity of the incident light on the edge of the aperture is 29.6% of the value at the center of the aperture. The resulting light distribution is one of a partial Gaussian beam profile which is perturbed by the scattering effects of the incident light field on the aperture itself. According to experimental measurements [19] and calculations using HVDT [4], the scattering modulations are strongest along the axis perpendicular to the incident light polarization, and weakest along the axis parallel to the incident light polarization, and the number of oscillations from the center of the aperture to the aperture edge is equal to the a/λ ratio.

Figure 5 shows the calculated values of the on-axis intensity around the focal plane (where $z_G = 0.01$ m) for various aperture sizes, normalized to the values of the peak intensity obtained in the absence of the aperture. The ratios of the aperture radius to the beam waist ω_a chosen are 0.16, 0.31, 0.5 and 1. These values were chosen as they illustrate calculations in the regime between the fully diffractive and the fully Gaussian regimes. The aperture radius is also expressed in multiples of the wavelength. In the diffraction regime, the location of the on-axis peak shifts with an increasing aperture radius and is located at an on-axis position of a^2/λ . In the Gaussian

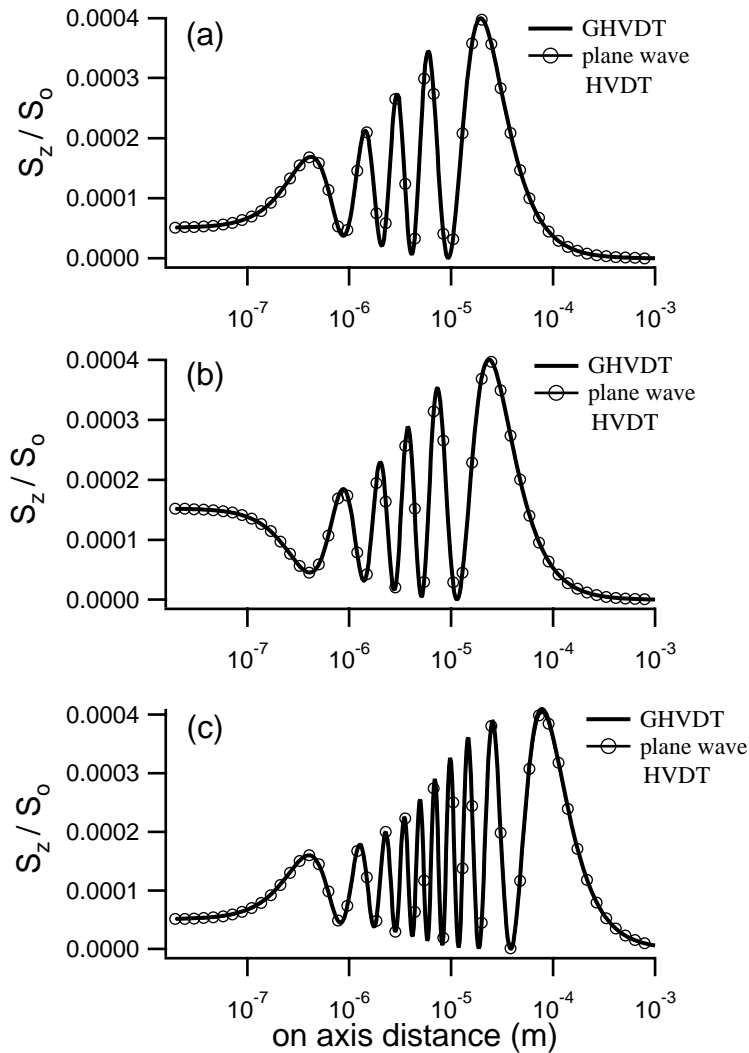


Fig. 3. Calculated plane-wave diffraction behavior using GHVDT. Calculations are of the normalized intensity versus on-axis distance from the aperture for aperture to wavelength ratios, a/λ , of (a) 5, (b) 5.5, and (c) 10. The incident peak intensity in the aperture plane is 10^{-4} , normalized to the theoretical peak intensity in the focal plane at $z = 0.01$ m. Calculated intensity distributions using a purely plane wave vector diffraction theory, HVDT, are included for comparison purposes.

beam propagation regime, the on-axis location of the peak intensity is constant and located in the focal plane. For the chosen laser parameters, these two values are equal when $a = 113\lambda$. As observed in Fig. 5, for values of $a < 113\lambda$ the peak on-axis intensity is shifted closer to the aperture plane, and for values of $a > 113\lambda$ the peak on-axis intensity remains at a distance of 1 cm from the aperture even as the aperture radius is increased. Also note that as the aperture radius is increased the peak intensity significantly grows in magnitude and axially narrows due to the increasing contribution of the focal properties of the incident converging beam.

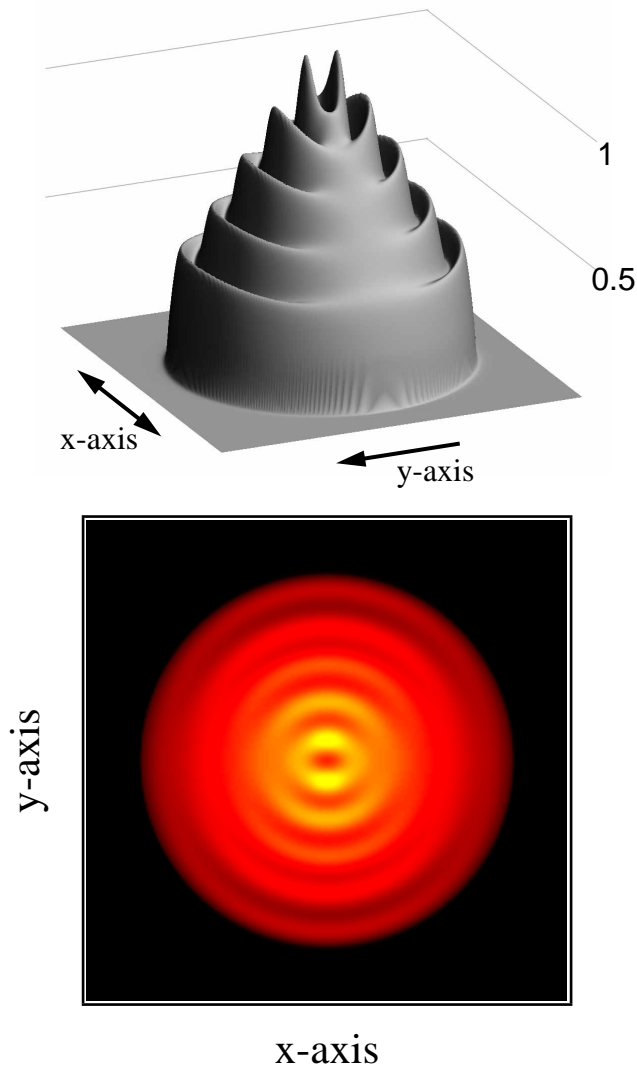


Fig. 4. Calculation of the z -component of the Poynting vector versus both x and y . Calculations are in the aperture plane for an incident Gaussian beam with the beam waist, ω_0 , in the aperture plane and an aperture radius of $a = 5\lambda = 0.78\omega_0$.

One of the important parameters of focused Gaussian laser beams is the maximum achievable intensity value. In the diffracted-Gaussian regime the maximum achievable intensity value of a converging clipped beam increases with an increasing aperture radius. This behavior is observed in Figs. (3) and (5) as the maximum normalized intensity increases by a factor of 1,000 from 4×10^{-4} for $a \ll \omega_a$ to 0.4 for a clipping ratio $a/\omega_a = 1$. Figure 6 is a calculation of the peak on-axis intensity as a function of the clipping ratio, for $z_G = 0.01$ m, and for a wide range of clipping ratios. The mathematical fit to the data calculated in Fig. 6 empirically follows that

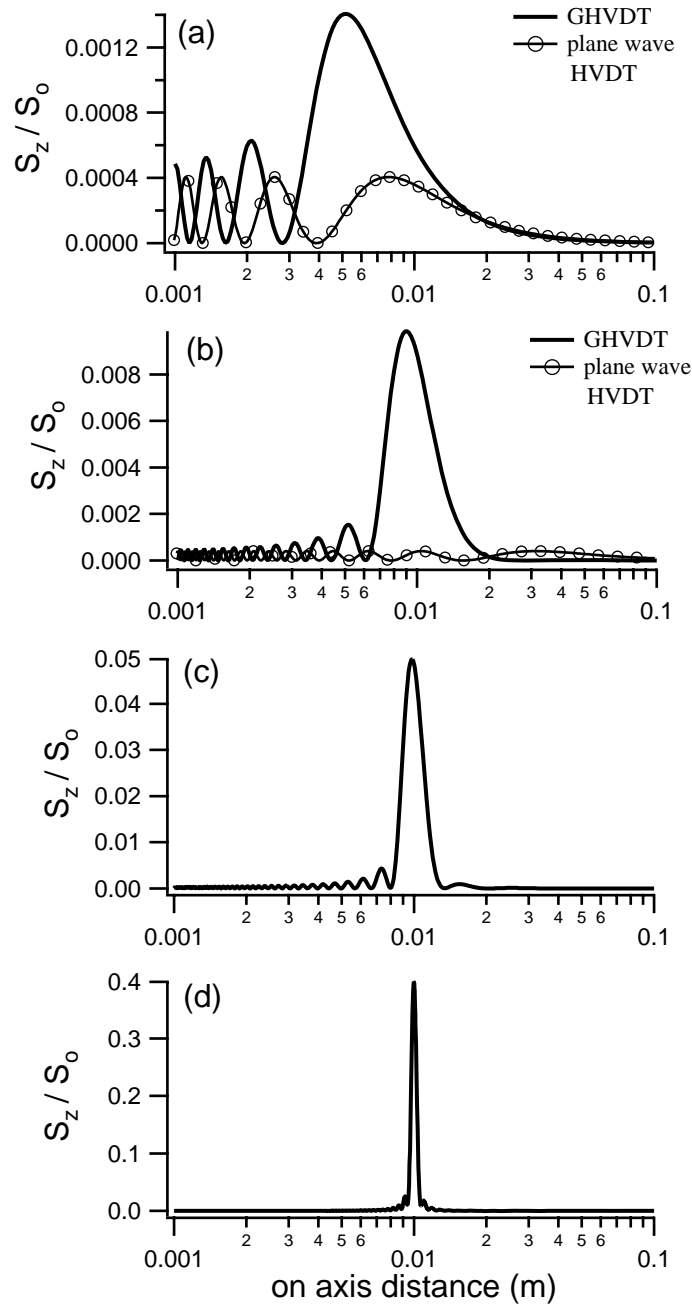


Fig. 5. Calculations of the normalized on-axis intensity for the regime between pure diffractive and pure Gaussian behavior for $z_G = 0.01$ m and (a) $a = 100\lambda = 0.16\omega_a$, (b) $a = 200\lambda = 0.31\omega_a$, (c) $a = 318\lambda = 0.5\omega_a$, and (d) $a = 636\lambda = \omega_a$. All intensities are normalized to the peak unperturbed focal spot intensity. Calculated intensity distributions using a purely plane wave vector diffraction theory, HVDT, are included to illustrate the transition of the GHVDT model from the diffraction regime to the focused diffracted-Gaussian regime.

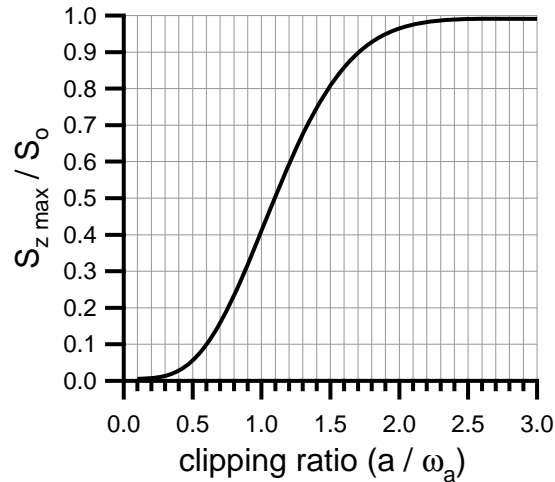


Fig. 6. Calculation of the maximum normalized intensity beyond the aperture as a function of the clipping ratio, a/ω_a , where $z_G = 0.01$ m.

of an error function, where

$$\frac{S_z}{S_0} = 0.49 + 0.50 \operatorname{erf} \left[-0.266 \left(\frac{a}{\omega_a} \right)^2 + 2.25 \frac{a}{\omega_a} - 2.14 \right]. \quad (28)$$

Another important parameter of focused Gaussian laser beams is the beam width in the focal plane. For unperturbed Gaussian beam propagation the minimum beam waist is commonly known as the transform-limited spot size. Figure 7 is a plot of the Gaussian width of the calculated intensity distribution in the focal plane as a function of the clipping ratio for a wide range of values from 0.01 to 3. For clipping ratios larger than 2, the minimum beam width in the focal plane asymptotically approaches that of the unperturbed minimum beam width. In the diffraction-Gaussian regime, the beam width in the focal plane is empirically found to follow a log-log relationship for clipping ratios less than ~ 0.6 , where for the parameters investigated here

$$\log \left(\frac{\omega}{\omega_0} \right) = -\log \left(\frac{a}{\omega_a} \right) + \log(1.33). \quad (29)$$

Figures 6 and 7, and Eqs. (28) and (29), can be used to predict the theoretical maximum intensity and theoretical minimum beam waist for a clipped focused Gaussian beam. For example, if an unperturbed Gaussian beam having a wavelength of 780 nm and a minimum spot size of $5 \mu\text{m}$ passes through an aperture located 1 cm before the focal spot with a diameter of 1 mm ($a/\omega_a = 1$) then the new theoretical maximum intensity would be 40% of that of a transform-limited Gaussian beam, and the new theoretical beam waist would be 46% wider than that of an unperturbed beam. If the aperture diameter is increased to 1.5 mm, then the theoretical maximum intensity would double to 80%, and the minimum beam waist would shrink to only 12.4% wider than that of a transform-limited beam.

4. Conclusions

A single theoretical model has been presented which can be used for: highly clipped Gaussian beams in the diffraction regime, unperturbed TEM₀₀ Gaussian propagation, as well as the

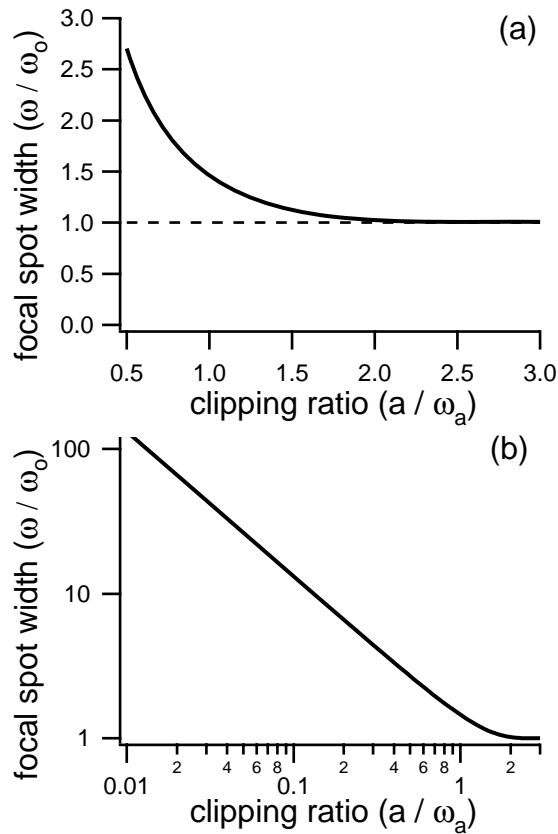


Fig. 7. Calculation of the e^{-2} width of the beam intensity profile in the focal plane as a function of the clipping ratio, a/ω_a , where $z_G = 0.01$ m.

diffracted-Gaussian regime in between the two extremes. Calculations in the highly clipped, or “plane wave”, diffractive regime show that the model reproduces expected near-field diffractive behavior including scattering effects in the aperture plane. Calculations with large clipping ratios, or “unperturbed” Gaussian beams, show that the model reproduces expected propagation behavior for focused TEM₀₀ Gaussian beams. In between, in the diffracted-Gaussian regime, calculations were performed for the maximum intensity beyond the aperture plane and the minimum beam width in the focal plane as a function of the clipping ratio. Calculations show that for a converging, clipped Gaussian beam the maximum attainable intensity beyond the aperture follows an error function of the clipping ratio, and the minimum beam width in the focal plane is found to have a log-log relationship to the clipping ratio.

Appendix A: Longitudinal field component in the paraxial approximation

The integral expressions for all the components of the electric and magnetic field provided in Eqs. (16) - (21) constitute the key results of this work. The integrals can be evaluated in analytic form in special cases, such as for on-axis ($x_1 = y_1 = 0$) or in the paraxial approximation (PA). Since an expression for the longitudinal component (E_z) of the electric field for focused Gaussian beams is not easily available in the literature, we provide here the expression in the

paraxial approximation for the unperturbed Gaussian propagation regime ($a \gg \omega_a$). The on-axis value of the longitudinal component is zero.

In the paraxial approximation, when ρ_1 occurs in the exponent, it can be simplified to

$$\rho_1 \approx p_1 z_1 + \frac{(x_1 - x_{01})^2 + (y_1 - y_{01})^2}{2p_1 z_1}. \quad (30)$$

For all occurrences of ρ_1 in the denominators, it is replaced by $p_1 z_1$. Under the paraxial approximation, the integral in Eq. (18) can be analytically evaluated, leading to

$$E_z(\vec{r}_1) = \frac{E_0 (1 + 3s_{11})}{4 p_1^3 z_1^2 d_1^2} (\kappa_1 + \kappa_2 + \kappa_3) e^{-ip_1^2 z_1} e^{-c_1(x_1^2 + y_1^2)}, \quad (31)$$

where

$$\kappa_1 = \frac{ax_1}{d_1^4} (b_1 - 2a_1) \quad (32)$$

$$\kappa_2 = \frac{ab_1 x_1}{d_1^4} \quad (33)$$

$$\kappa_3 = \frac{bx_1}{d_1^2} \left[\frac{aa_1^2}{d_1^4} (x_1^2 + y_1^2) + b \right] \quad (34)$$

$$s_{11} = \frac{1}{ip_1^2 z_1} \left(1 + \frac{1}{ip_1^2 z_1} \right) \quad (35)$$

with

$$a = \frac{i}{2(1 + 2iz_{G1})(q_1 - z_{G1})^2} \quad (36)$$

$$b = -\frac{1}{1 + 2iz_{G1}} \left(\frac{1}{q_1 - z_{G1}} + ip_1^2 \right) \quad (37)$$

$$a_1 = \frac{i}{2z_1} \quad (38)$$

$$b_1 = \frac{i}{2(q_1 - z_{G1})} \quad (39)$$

$$c_1 = \frac{a_1 b_1}{a_1 + b_1} \quad (40)$$

and

$$d_1 = \sqrt{(a_1 + b_1)}. \quad (41)$$